ChemPubSoc Europe

DOI: 10.1002/cphc.201701380

CHEMPHYSCHEM Articles

Grain Size Modulation and Interfacial Engineering of $CH_3NH_3PbBr_3$ Emitter Films through Incorporation of Tetraethylammonium Bromide

Nur Fadilah Jamaludin,[a, b, c] Natalia Yantara,[a] Yan Fong Ng,[a, b, c] Mingjie Li,[d] Teck Wee Goh,[d] Krishnamoorthy Thirumal,[a] Tze Chien Sum,[d] Nripan Mathews,[a, c] Cesare Soci,[d] and Subodh Mhaisalkar*[a, c]

Metal halide perovskites have demonstrated breakthrough performances as absorber and emitter materials for photovoltaic and display applications respectively. However, despite the low manufacturing cost associated with solution-based processing, the propensity for defect formation with this technique has led to an increasing need for defect passivation. Here, we present an inexpensive and facile method to remedy surface defects through a postdeposition treatment process using branched alkylammonium cation species. The simultaneous realignment of interfacial energy levels upon incorporation of tetraethylammonium bromide onto the surface of $CH_3NH_3PbBr_3$ films contributes favorably toward the enhancement in overall light-emitting diode characteristics, achieving maximum luminance, current efficiency, and external quantum efficiency values of 11 000 cd m^{-2}, 0.68 cd A^{-1}, and 0.16 %, respectively.

1. Introduction

Initially shown to be an alternative to dyes in dye-sensitized solar cells,[1] hybrid halide perovskites have since evolved to be a wonder material for various optoelectronic applications.[2] Offering a wide spectrum of unique characteristics,[2–6] it is unsurprising this material has since attracted widespread attention. Within a short span of five years, not only have perovskites found their way into the field of lighting and displays[7] but also charted an unprecedented rise in efficiency to emerge as a promising solid-state lighting technology.[8–12]

[a] N. F. Jamaludin, Dr. N. Yantara, Y. F. Ng, K. Thirumal, Prof. N. Mathews, Prof. S. Mhaisalkar
Energy Research Institute @ NTU (ERI@N)
Nanyang Technological University
Research Techno Plaza, X-Frontier Block, Level 5,
50 Nanyang Drive, Singapore 637553 (Singapore)
E-mail: subodh@ntu.edu.sg

[b] N. F. Jamaludin, Y. F. Ng
Interdisciplinary Graduate School
Nanyang Technological University
50 Nanyang Avenue, Singapore 639798 (Singapore)

[c] N. F. Jamaludin, Y. F. Ng, Prof. N. Mathews, Prof. S. Mhaisalkar
School of Materials Science and Engineering
Nanyang Technological University
50 Nanyang Avenue
Singapore 639798 (Singapore)

[d] Dr. M. Li, T. W. Goh, Prof. T. C. Sum, Prof. C. Soci
Division of Physics and Applied Physics, School of Physical and Mathematical Sciences
Nanyang Technological University
21 Nanyang Link, Singapore 637371 (Singapore)

Supporting Information and the ORCID identification number(s) for the author(s) of this article can be found under https://doi.org/10.1002/cphc.201701380.

Despite boasting cheap solution-based processing, the tendency for defect formation with this technique necessitates studies focusing on passivation of these electrical shunt pathways in perovskite solar cells.[13–15] This is further exacerbated by the propensity for degradation or phase segregation[16] during postdeposition annealing. Not only does it result in changes to surface properties, but more importantly, lead to under-coordination of surface Pb atoms to the detriment of device performance.[17] Other than acting as sites for non-radiative recombination, under-coordination of surface elements also expedites film degradation due to the increased susceptibility to the adsorption of other species for charge neutralization.[18] Moreover, thermally-induced grain growth may also introduce defect states within the system owing to the formation of unconnected grains.[19] Poor device performance arising from charge trapping at interfaces[20] have fueled investigation into non-radiative loss reductions, which include incorporation of excess precursor material in the perovskite solution,[21] solvent engineering processes[22] and even through layering of passivating materials to inhibit moisture and oxygen permeation.[18,23] However, these methods have only shown limited success. The introduction of excess precursor material resulted in higher hysteresis due to the increased effect of ionic migration under device operation[24,25] whereas too thick a passivation layer can have adverse effect on device performance ensuing from reduced carrier injection efficacy.[26,27]

Herein, it is shown that by incorporating a quaternary ammonium compound—tetraethylammonium bromide (TEABr)—into methylammonium lead bromide ($MAPbBr_3$) through a facile postdeposition step, grain size modulation and passivation of surface defects; as evidenced by the increased photolu-

minescence (PL) quantum yield (PLQY) and improved stoichiometry of surface elements, provide the driving force for enhancement in both film and device characteristics. An additional advantage manifests in the form of energy level realignment at the charge selective interfaces which also reduces the carrier injection barrier into the emitter layer and in turn, minimizes series resistance.

2. Results and Discussion

While the reference $MAPbBr_3$ film was prepared using a solvent engineering technique as described in the Experimental Section, the other samples were subjected to an additional postdeposition treatment using TEABr solutions of varying concentrations (10, 15, and 20 mg mL^{-1}). Figure 1a presents the XRD patterns of the reference (0 mg mL^{-1}) and TEABr-treated films as well as that of the powder obtained from drying an equimolar solution of TEABr and $PbBr_2$. While the XRD patterns of all films exhibit characteristic $CH_3NH_3PbBr_3$ peaks with preferred orientation in the (100) plane, treatment of films with various TEABr concentrations saw the presence of additional peaks at 2θ values of 9.62° and 16.92°, corresponding to reflections from the TEABr-based compound. This suggests the co-existence of two separate phases in the resulting film; in line with reports of lower dimensional perovskites forming on introduction of bulkier cation groups.[28,29] It is interesting to note that although the passivating properties of similar chemicals have been reported for the iodide[18] and bromide[30] systems, neither highlighted the presence of reflection below $2\theta = 10°$, indicative of a lower dimensional phase.[31] The increasing ratio of peak intensities between peak positions 9.62° and 14.94° with higher TEABr concentration translates to the increasing proportion of this secondary phase in the film. Analysis of nuclear magnetic resonance (NMR) spectra (Figure S1 in the Supporting Information) acquired for the reference and 10 mg mL^{-1} TEABr-treated films revealed presence of characteristic TEABr peaks in the latter, providing further evidence of its incorporation during the postdeposition treatment.

Figure 1b shows the optical absorbance spectra of the reference and TEABr-treated films. Decrease in absorbance and presence of an excitonic feature at 325 nm with increasing TEABr concentration are accrued to the formation of a lower dimensional phase in the resulting film. This is in good agreement with the XRD phase analysis, where introduction of a bulky cation species such as the tetraethylammonium cation, into the 3D perovskite framework saw peaks at lower 2θ values, consistent with the presence of a secondary compound. The normalized PL spectra, as presented in Figure 1c, revealed no change in peak emission position (538 nm) with increasing TEABr concentration, implying the non-emissive nature of the lower dimensional phase. This is further confirmed through excitation spectra (Figure S2) measurements where no increase in PL intensity was noted within the absorption range of the secondary phase. The single peak emission

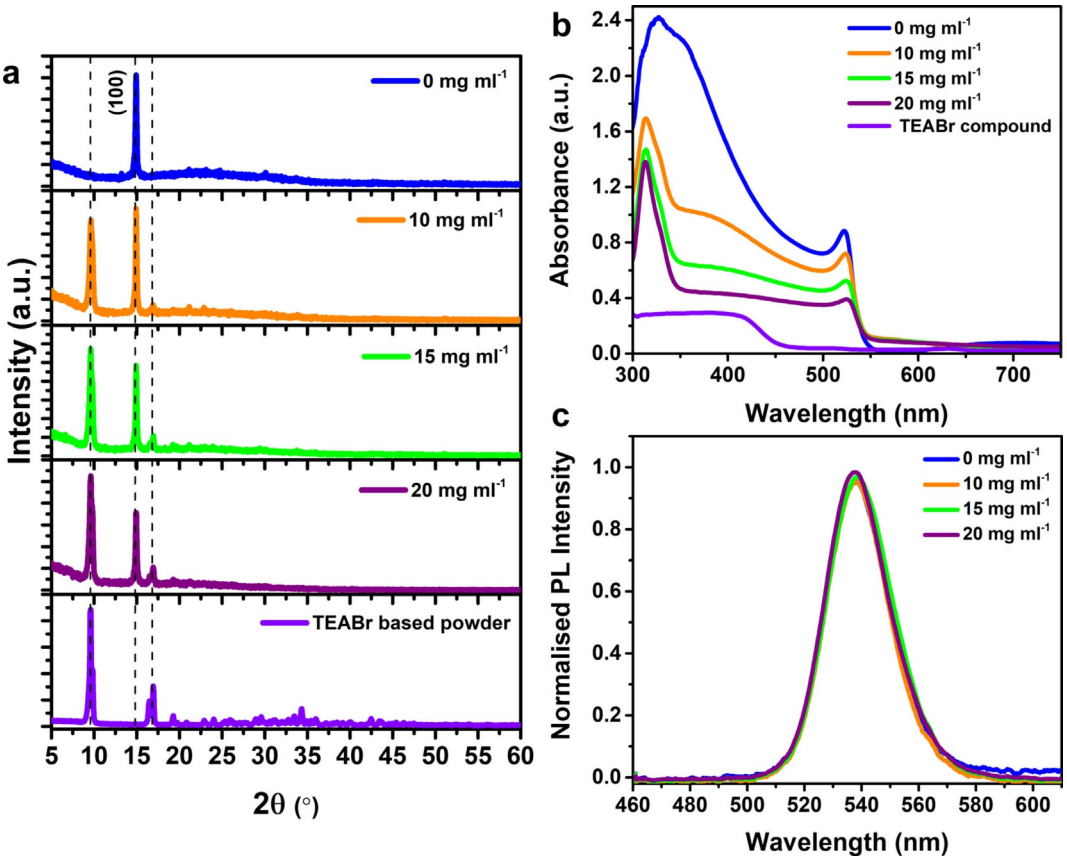

Figure 1. a) XRD pattern b) UV/Vis absorption, and c) normalized PL spectra of reference (0 mg mL^{-1}) and TEABr-treated samples with varying concentrations of TEABr ranging from 10 to 20 mg mL^{-1}.

observed for all films eliminates energy funneling[32] as a possible mechanism for the notable PL enhancement (discussed subsequently) whereas the PL full width at half maximum (FWHM) too remains at ≈24 nm, unaffected by TEABr concentration. Computation of PL quantum yield (PLQY) values was carried out for absorbance-corrected fluorimetric determination of the films (Table 1). It is conspicuous that increasing the

Table 1. Summary of the optical and photophysical properties of the reference and TEABr-treated films.

TEABr concentration [mg mL^{-1}]	λ [nm]	FWHM [nm]	PLQY [%]	τ_{PL} [ns]	τ_{rad} [ns]	$\tau_{non\text{-}rad}$ [ns]
0	538	24	1.2	2.1	175	2.13
10	538	24	6.6	10.7	162	11.5
15	538	24	11.5	17.4	151	19.7
20	538	24	12.6	22.4	178	25.6

TEABr concentration led to increased fluorescence, with 20 mg mL^{-1} showcasing more than ten-fold enhancement in PLQY value as compared to the reference. The systematic improvement to fluorescence is due to surface defect passivation on treating the films with TEABr. To verify this, X-ray photoelectron spectroscopy (XPS) was done to determine the surface elemental stoichiometry for the reference and 20 mg mL^{-1} TEABr-treated films (Figure S3), corresponding to the extremities of the measured PLQY values. It was found that the atomic ratio Br/Pb on the surface of the un-passivated film is 2.5, indicative of Br deficiency, whereas after post-treatment with TEABr, the Br/Pb ratio increases toward the stoichiometric ratio of 3.0. This suggests that the TEABr treatment allows surface Br vacancies to be filled and Pb atoms to be more coordinated, thus demonstrating its beneficial effect in remedying surface defects.

In view of the higher PLQY values observed with increasing TEABr concentration, other photophysical studies were executed to investigate the correlation between TEABr concentration and film properties. The valence and conduction energy band levels with respect to vacuum were derived from photoelectron spectroscopy in air (PESA) measurements whereas the band gap values were estimated from the absorbance spectra (Figure S4). In this case, Tauc plot was not employed in the band gap determination, rather, the Elliot model for optical absorption by exciton was used to deconvolute the excitonic feature present near the absorption edge to provide a more accurate representation of the optical band gap (Table S1).[33] It was deduced that TEABr treatment has negligible effect on the electronic band gap despite the notable shifts in energy levels. The change in band energy alignment is also supported by the binding energy shift of Br 3d peak toward lower binding energy (from 69.0 ± 0.1 to 68.6 ± 0.1 eV) in XPS on treating the film with 20 mg mL^{-1} of TEABr, as it is known that the valence band maximum is mainly contributed by the 4p state of Br (Figure S3).[34] From the band diagram (Figure S5), the valence band was found to shift toward vacuum with incorporation of TEABr, regardless of the concentration used. This implies a reduction in energy barrier between the hole-transport material and perovskite, allowing for better matching of interfacial energy levels and enabling more effective charge injection. The effect of TEABr concentration was also probed through PL decay measurements (Figure S6). The PL decay curves were fitted with a bi-exponential decay function to extract the amplitude weighted average lifetimes (τ_{PL}). The fast and slow decay constants are attributed to the recombination of excitons in the defect-rich regions (e.g., near grain surfaces) and the defect-poor regions (e.g., inside the grains), respectively. The average PL lifetime of the reference was found to be τ_{PL} ≈2.1 ns whereas the TEABr-treated samples gave progressively longer lifetimes with the 20 mg mL^{-1} TEABr-treated sample yielding τ_{PL} ≈22.4 ns (Table 1). This concurs with the XPS data where passivation of surface defects through TEABr treatment not only improves the stoichiometry of surface Br/Pb ratio, but also reduces surface traps. Based on the correlation between the PLQY and PL decay lifetimes,[35] τ_{rad} and $\tau_{non\text{-}rad}$ were calculated. It was noted that τ_{rad} decreases from 175 ns in the reference to 151 ns in the 15 mg mL^{-1} TEABr-treated sample. The $\tau_{non\text{-}rad}$, on the other hand, shows systematic increase (i.e. decrease of non-radiative recombination rates) with TEABr concentration which is accordant with the reduction of surface defects.

Figure 2 shows the top and cross-section secondary electron images (SEI) of the reference $MAPbBr_3$ and TEABr-treated films taken using field emission scanning electron microscope. While the reference film shows a smooth surface consisting of fused

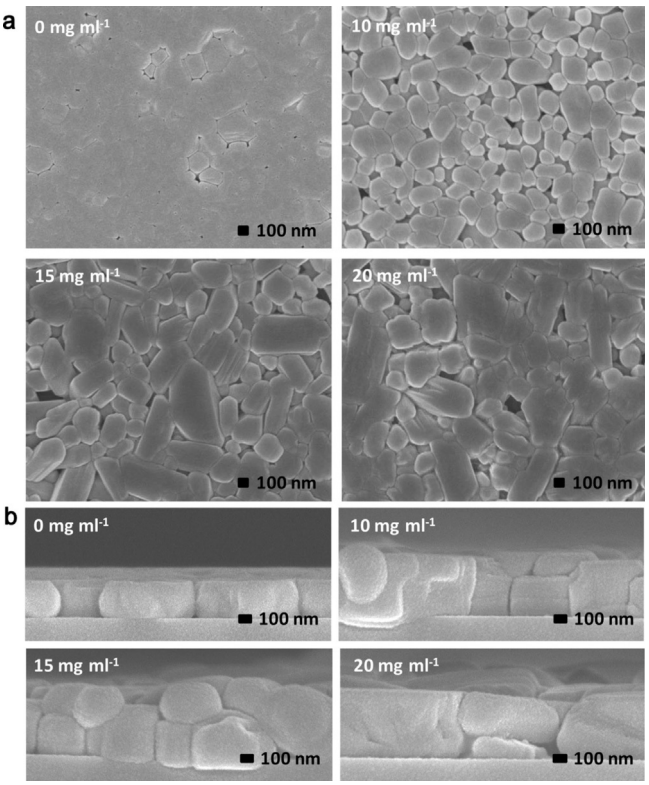

Figure 2. a) Top and b) cross-section images of reference $MAPbBr_3$ (0 mg mL^{-1}) and TEABr-treated samples with varying concentrations of TEABr ranging from 10 to 20 mg mL^{-1}.

grains, with TEABr treatment however, the films become progressively rougher as noted by the appearance of more defined grains (Figure 2a). As compared to the columnar grains in the single layered reference film, all TEABr-treated films formed a bilayer stack consisting of small, globular grains (Figure 2b). It is postulated that the smaller grains for the TEABr-treated films, evident in the cross-section images, contribute significantly toward the higher PLQY values. This is in congruence with published reports where spatial confinement facilitates radiative recombination of charges in perovskites.[12,35] It needs to be emphasized that in this case, the grain's thickness, rather than its width, is used as a basis for comparison due to the vertical manner of charge injection during device operation. From the plots of grain thickness and PLQY values against TEABr concentration (Figure S7), it is curious that although grain thickness increases for concentration beyond 15 mg mL^{-1}, PLQY value did not suffer. This however, can be explained by the higher proportion of lower dimensional phase formed in the film offering a confined low dimensional quantum well structure,[36] which facilitates radiative recombination process. All in all, it can be concluded that the grain size effect dominates at lower concentrations of TEABr but the lower dimensional phase effect (quantum well structure) plays a more critical role in carrier confinement at higher TEABr concentrations. Despite the higher PLQY value achieved, the increase in secondary phase content may result in lower conductivity of the perovskite film, which can consequently affect device performance.

The samples were also imaged using backscattered electron mode to determine the phase distribution in the films (Figure S8). However, no significant difference in contrast was observed, plausibly due to the negligible variance in the elemental content of the two phases. It is hypothesized that the post-deposition treatment with TEABr passivates both the surface vacancy and grain boundary defects present in the film.[37] The annealing step carried out subsequently, provides the driving force for diffusion of the ions into the deeper layers resulting in the formation of a bi-layered mixed-dimensional perovskite phase as seen by the XRD pattern. As opposed to the reference, the TEABr-treated films too saw a 50% increase in thickness independent of TEABr concentration attributed to incorporation of bulky tetraethylammonium ions into the $MAPbBr_3$ framework. In order to affirm that the overall enhancement to the optoelectronic properties of the TEABr-treated films arose solely from TEABr incorporation, topographical assessment of the untreated and isopropanol (IPA) treated films was carried out (Figure S9), where no change in morphology was observed on treating the reference film surface with IPA.

To correlate the film properties with device performance, perovskite-based light-emitting diodes (PeLEDs) were subsequently fabricated. The device architecture adopted and overall performance are as shown in Figure 3a and Figure 3b –d respectively. From the Figure, progressive increase in maximum luminance with TEABr concentration was noted, from 20 cd m^{-2} in the reference $MAPbBr_3$ device to a maximum value of 11 000 cd m^{-2} for the 15 mg mL^{-1} device. Beyond this concentration, device performance starts to deteriorate. Lower

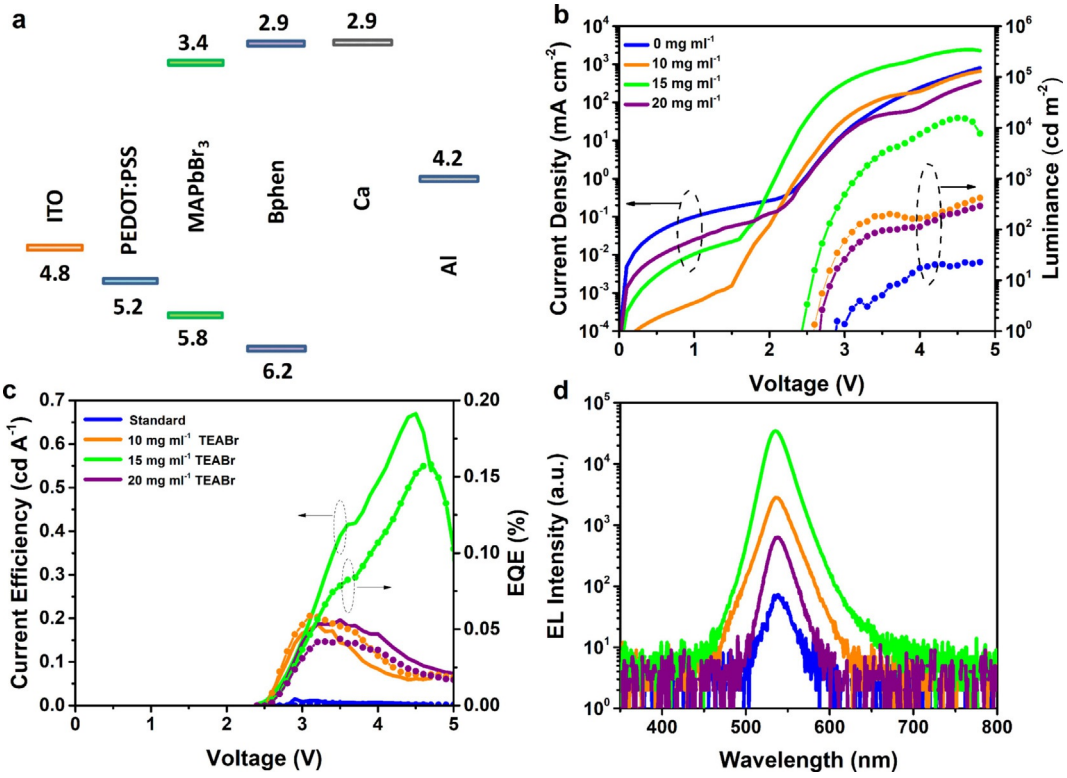

Figure 3. a) Schematic of device architecture, b) current density (*J*), luminance (*L*) against voltage (*V*) curves, c) current efficiency *(CE)* against voltage *(V)* curve, and d) electroluminescence spectra at 4 V for reference (0 mg mL^{-1}) and TEABr-treated samples with varying concentrations of TEABr ranging from 10 to 20 mg mL^{-1}.

threshold voltage was also observed, dropping from 3 V in the reference device to 2.4 V in the 15 mg mL^{-1} TEABr-treated device. The higher efficiencies observed coincided with increased luminance levels. The most efficient device was achieved with 15 mg mL^{-1} TEABr treatment, reaching a current efficiency andexternal quantum efficiency (EQE) of 0.68 cd A^{-1} and 0.16% respectively, which is approximately a hundred-fold improvement as compared to the reference device (0.0018%). The enhancement in device performance is attributed to three phenomena: a) increased radiative recombination through spatial charge confinement, b) reduction in surface defect density and c) lowering of energetic barrier at the interface due to improved energy level matching, thereby allowing for more efficient carrier injection into the emitter layer. The lower current turn-on observed also attests to the improved injection offered with TEABr treatment. Although the energy band levels of the TEABr-treated films are similar, the threshold voltage increased with higher TEABr concentration (20 mg mL^{-1}). This stems from the excessive amount of lower dimensional phase present in the film which limits charge conduction across the perovskite emitter and in turn contributes towards poorer device efficiency.

To rule out the influence of emitter thickness on device performance, PeLEDs with emitter thickness comparable to the TEABr-treated films were fabricated by increasing the concentration of the perovskite precursor solution to 1.2 M (Figure S10). Despite the slight improvement in luminance and current efficiency offered by the thicker device (Figure S11), the 15 mg mL^{-1} TEABr-treated device still reigns supreme. This provides strong evidence that TEABr treatment is the main contributor toward the overall enhancement in device performance.

3. Conclusions

It was shown that through an inexpensive and facile postdeposition treatment process using tetraethylammonium bromide (TEABr), the performance of methylammonium lead bromide ($MAPbBr_3$)-based perovskite-based light-emitting diodes (PeLEDs) can be greatly improved. The mixed dimensional perovskite formed on TEABr treatment, evidenced by the presence of reflections at lower 2θ values, indicate that the secondary phase plays a role in the enhancement of overall device performance. While the absence of emission in the excitation spectra corresponding to the absorption edge at 325 nm eliminates energy funneling as the mechanism for improved performance, it does not discount the plausibility that grain size modulation is crucial for optimum intercalation of the two phases. Not only did the TEABr treatment resolve the issue of non-stoichiometric ratio of surface elements, the simultaneous improvement in morphology and tailoring of the energy band levels at the charge selective interfaces have also allowed for more efficient injection and radiative recombination of charge carriers, as supported by the substantial enhancement in both film optical properties and device performance. This provides strong evidence that contributions from these factors can also lead to enhanced photoluminescence and electroluminescence despite absence of energy funneling. This crucial discovery is not only testament to the need for stringent defect management in perovskite film deposition but may very well present a new opportunity for further research into mixed dimensional systems as effective emitters for PeLEDs.

Experimental Section

The devices were made on indium-doped tin oxide (ITO, 7 Ω sq^{-1}) coated glass substrates. The substrates were cleaned sequentially using decon soap, deionised water and ethanol. This was then followed by drying and plasma treatment for 15 mins. PEDOT:PSS (Clevios P VP Al 4083) was spin-coated at 4000 rpm for 30 s and annealed for 30 min at 130 °C. The $MAPbBr_3$ solution was synthesized with equimolar ratio of MABr (Dyesol) and $PbBr_2$ (Aldrich, 99.999%) dissolved in DMF/DMSO cosolvent (3:1) (1 M) and used as-prepared for all subsequent spin-coating steps. The reference film was spin-coated at 5000 rpm for 12 s with toluene dripped at 4 s from the start of the spin-coating process. Thereafter, the films were then annealed at 100 °C for 30 min. The TEABr solution of various concentrations (10, 15, and 20 mg mL^{-1} in IPA) was allowed to settle on the film for 15 s before spin-coating at 4000 rpm for 30 s. The films were then annealed again at 100 °C for 10 min. Bathophenanthroline (BPhen) (Aldrich, 97%) (25 nm), calcium (10 nm) and aluminum (100 nm) were finally thermally evaporated to form the electron transporting layer and cathode, respectively. The evaporation was carried out under high vacuum ($< 1 \times 10^{-6}$ mbar) and thereafter encapsulated prior to testing. The final cell size was measured to be 7 mm^2.

All device characterizations were carried out in ambient conditions. The device characteristics (*J–V–L*) and electroluminescence spectra were collected using a Keithley 2612B source meter and an Ocean-Optics QE Pro spectrometer connected to an integrating sphere, operated using LabVIEW. Optical absorption measurements were carried out using a UV/Vis-NIR Shimadzu UV-3600 spectrofluorophotometer with an integrating sphere attachment. PL spectra was obtained using Fluoromax-4 (Horiba Jobin Yvon) spectrofluorometer at an excitation wavelength of 400 nm. Time-resolved PL was carried out with streak camera system (Optronis Optoscope™), with the 400 nm pump pulse obtained by frequency-doubling of 800 nm pulse from the regenerative amplifier (Coherent Libra, pulse width 50 fs, repetition rate 1 kHz) with a BBO crystal. The absolute PLQY was measured using a calibrated integrating sphere under the 400 nm fs laser excitation. XPS measurements were performed using a hemispherical electron analyser (Omicron EA-125). The X-ray used was Al Kα line (1486.6 eV) and the measurement was collected at either 50.0 eV (wide scans) or 20.0 eV (elemental scans) pass energy. The atomic ratios were derived by taking the ratio of areas of the Br 3d and Pb 4f peaks, taking into account the atomic sensitivity factor. All morphological and cross-section imaging were done with a field emission scanning electron microscope (JEOL JSM-7600F), whereas the X-ray diffraction patterns were obtained using XRD Bruker D8 Advance.

Acknowledgements

We would like to extend our gratitude to Dr. Tom Baikie for the valuable discussion on the obtained XRD data. This research was supported by the National Research Foundation, Prime Minister's Office, Singapore under its Competitive Research Programme (CRP Award No. NRF-CRP14-2014-03) and through the Singapore-

Berkeley Research Initiative for Sustainable Energy (SinBeRISE) CREATE Program.

Conflict of interest

The authors declare no conflict of interest.

Keywords: $CH_3NH_3PbBr_3$ · hybrid halide perovskites · light-emitting diodes · mixed dimensional systems · postdeposition treatment

[1] S. P. Singh, P. Nagarjuna, *Dalton Trans.* **2014**, *43*, 5247 – 5251.
[2] Q. Chen, N. De Marco, Y. Yang, T.-B. Song, C.-C. Chen, H. Zhao, Z. Hong, H. Zhou, Y. Yang, *Nano Today* **2015**, *10*, 355 – 396.
[3] P. P. Boix, K. Nonomura, N. Mathews, S. G. Mhaisalkar, *Mater. Res. Materials Today* **2014**, *17*, 16 – 23.
[4] Q. Dong, Y. Fang, Y. Shao, P. Mulligan, J. Qiu, L. Cao, J. Huang, *Science* **2015**, *347*, 967 – 970.
[5] G. Xing, N. Mathews, S. Sun, S. S. Lim, Y. M. Lam, M. Grätzel, S. Mhaisalkar, T. C. Sum, *Science* **2013**, *342*, 344 – 347.
[6] J. Berry, T. Buonassisi, D. A. Egger, G. Hodes, L. Kronik, Y.-L. Loo, I. Lubomirsky, S. R. Marder, Y. Mastai, J. S. Miller, et al., *Advanced Materials* **2015**, *27*, 5102 – 5112.
[7] Y.-H. Kim, H. Cho, T.-W. Lee, *Proc. Natl. Acad. Sci. USA* **2016**, *113*, 11694 – 11702.
[8] J. Li, X. Shan, S. G. R. Bade, T. Geske, Q. Jiang, X. Yang, Z. Yu, *J. Phys. Chem. Letters* **2016**, *7*, 4059 – 4066.
[9] M. J. Yuan, L. N. Quan, R. Comin, G. Walters, R. Sabatini, O. Voznyy, S. Hoogland, Y. B. Zhao, E. M. Beauregard, P. Kanjanaboos, et al., *Nat. Nanotechnol.* **2016**, *11*, 872 – 877.
[10] L. Zheng, D. Zhang, Y. Ma, Z. Lu, Z. Chen, S. Wang, L. Xiao, Q. Gong, *Dalton Transactions* **2015**, *44*, 10582 – 10593.
[11] Y.-H. Kim, H. Cho, J. H. Heo, T.-S. Kim, N. Myoung, C.-L. Lee, S. H. Im, T.-W. Lee, *Advanced Materials* **2015**, *27*, 1248 – 1254.
[12] H.-K. Seo, H. Kim, J. Lee, M.-H. Park, S.-H. Jeong, Y.-H. Kim, S.-J. Kwon, T.-H. Han, S. Yoo, T.-W. Lee, *Adv. Mater.* **2017**, *29*, 1605587.
[13] A. Abate, M. Saliba, D. J. Hollman, S. D. Stranks, K. Wojciechowski, R. Avolio, G. Grancini, A. Petrozza, H. J. Snaith, *Nano Letters* **2014**, *14*, 3247 – 3254.
[14] Y. Shao, Z. Xiao, C. Bi, Y. Yuan, J. Huang, *Nat. Commun.* **2014**, *5*, 5784.
[15] B. Wang, K. Y. Wong, S. Yang, T. Chen, *J. Mater. Chem. A* **2016**, *4*, 3806 – 3812.
[16] H. Xie, X. Liu, L. Lyu, D. Niu, Q. Wang, J. Huang, Y. Gao, *J. Phys. Chem. C* **2016**, *120*, 215 – 220.
[17] N. K. Noel, A. Abate, S. D. Stranks, E. S. Parrott, V. M. Burlakov, A. Goriely, H. J. Snaith, *ACS Nano* **2014**, *8*, 9815 – 9821.
[18] S. Yang, Y. Wang, P. Liu, Y.-B. Cheng, H. J. Zhao, H. G. Yang, *Nat. Energy* **2016**, *1*, 15016.
[19] B.-E. Cohen, L. Etgar, *Frontiers of Optoelectronics* **2016**, *9*, 44 – 52.
[20] T. Tachikawa, I. Karimata, Y. Kobori, *J. Phys. Chem. Lett.* **2015**, *6*, 3195 – 3201.
[21] H. Cho, S.-H. Jeong, M.-H. Park, Y.-H. Kim, C. Wolf, C.-L. Lee, J. H. Heo, A. Sadhanala, N. Myoung, S. Yoo, et al., *Science* **2015**, *350*, 1222 – 1225.
[22] P. C. Harikesh, H. K. Mulmudi, B. Ghosh, T. W. Goh, Y. T. Teng, K. Thirumal, M. Lockrey, K. Weber, T. M. Koh, S. Li, S. Mhaisalkar, N. Mathews, *Chemistry of Materials* **2016**, *28*, 7496 – 7504.
[23] B. Chaudhary, A. Kulkarni, A. K. Jena, M. Ikegami, Y. Udagawa, H. Kunugita, K. Ema, T. Miyasaka, *ChemSusChem* **2017**, *10*, 2473 – 2479.
[24] S. Meloni, T. Moehl, W. Tress, M. Franckevičius, M. Saliba, Y. H. Lee, P. Gao, M. K. Nazeeruddin, S. M. Zakeeruddin, U. Rothlisberger, M. Grätzel, *Nat. Commmun.* **2016**, *7*, 10334.
[25] Y. Cheng, H.-W. Li, J. Qing, Q.-D. Yang, Z. Guan, C. Liu, S. H. Cheung, S. K. So, C.-S. Lee, S.-W. Tsang, *Journal of Materials Chemistry A* **2016**, *4*, 12748 – 12755.
[26] G. Li, Z.-K. Tan, D. Di, M. L. Lai, L. Jiang, J. H.-W. Lim, R. H. Friend, N. C. Greenham, *Nano Letters* **2015**, *15*, 2640 – 2644.
[27] S. Lee, J. H. Park, B. R. Lee, E. D. Jung, J. C. Yu, D. Di Nuzzo, R. H. Friend, M. H. Song, *J. Phys. Chem. Letters* **2017**, *8*, 1784 – 1792.
[28] D. H. Cao, C. C. Stoumpos, O. K. Farha, J. T. Hupp, M. G. Kanatzidis, *J. Am. Chem. Soc.* **2015**, *137*, 7843 – 7850.
[29] I. C. Smith, E. T. Hoke, D. Solis-Ibarra, M. D. McGehee, H. I. Karunadasa, *Angew. Chem. Int. Ed.* **2014**, *53*, 11232 – 11235; *Angew. Chem.* **2014**, *126*, 11414 – 11417.
[30] R. Naphade, B. Zhao, J. M. Richter, E. Booker, S. Krishnamurthy, R. H. Friend, A. Sadhanala, S. Ogale, *Advanced Materials Interfaces* **2017**, *4*, 1700562.
[31] M. Safdari, P. H. Svensson, M. T. Hoang, I. Oh, L. Kloo, J. M. Gardner, *J. Mater. Chem. A* **2016**, *4*, 15638 – 15646.
[32] Y. F. Ng, S. A. Kulkarni, S. Parida, N. F. Jamaludin, N. Yantara, A. Bruno, C. Soci, S. Mhaisalkar, N. Mathews, *Chemical Communications* **2017**, *53*, 12004 – 12007.
[33] R. J. Elliott, *Phys. Rev.* **1957**, *108*, 1384 – 1389.
[34] J. Endres, D. A. Egger, M. Kulbak, R. A. Kerner, L. Zhao, S. H. Silver, G. Hodes, B. P. Rand, D. Cahen, L. Kronik, A. Kahn, *J. Phys. Chem. Letters* **2016**, *7*, 2722 – 2729.
[35] Y. F. Ng, N. F. Jamaludin, N. Yantara, M. Li, V. K. R. Irukuvarjula, H. V. Demir, T. C. Sum, S. Mhaisalkar, N. Mathews, *ACS Omega* **2017**, *2*, 2757 – 2764.
[36] R. K. Misra, B.-E. Cohen, L. Iagher, L. Etgar, *ChemSusChem* **2017**, *10*, 3712 – 3721.
[37] T. Zhao, C.-C. Chueh, Q. Chen, A. Rajagopal, A. K. Y. Jen, *ACS Energy Lett.* **2016**, *1*, 757 – 763.

Manuscript received: December 28, 2017
Accepted manuscript online: January 3, 2018
Version of record online: February 27, 2018